

BRIEF DEFINITIVE REPORT

Hepatic FGF21 preserves thermoregulation and cardiovascular function during bacterial inflammation

Sarah C. Huen¹, Andrew Wang^{2,3}, Kyle Feola¹, Reina Desrouleaux^{2,3}, Harding H. Luan³, Richard Hogg¹, Cuiling Zhang^{2,3}, Qing-Jun Zhang⁴, Zhi-Ping Liu⁴, and Ruslan Medzhitov^{3,5}

Sickness behaviors, including anorexia, are evolutionarily conserved responses to acute infections. Inflammation-induced anorexia causes dramatic metabolic changes, of which components critical to survival are unique depending on the type of inflammation. Glucose supplementation during the anorectic period induced by bacterial inflammation suppresses adaptive fasting metabolic pathways, including fibroblast growth factor 21 (FGF21), and decreases survival. Consistent with this observation, FGF21-deficient mice are more susceptible to mortality from endotoxemia and polybacterial peritonitis. Here, we report that increased circulating FGF21 during bacterial inflammation is hepatic derived and required for survival through the maintenance of thermogenesis, energy expenditure, and cardiac function. FGF21 signaling downstream of its obligate coreceptor, β-Klotho (KLB), is required in bacterial sepsis. However, FGF21 modulates thermogenesis and chronotropy independent of the adipose, forebrain, and hypothalamus, which are operative in cold adaptation, suggesting that in bacterial inflammation, either FGF21 signals through a novel, undescribed target tissue or concurrent signaling of multiple KLB-expressing tissues is required.

Introduction

Physiobehavioral responses to infection such as anorexia are part of a collection of sickness behaviors that are evolutionarily conserved (Murray and Murray, 1979; Adamo, 2005; Ayres and Schneider, 2009). Anorexia of acute illness has traditionally been considered maladaptive in the face of a presumed hypercatabolic state. However, anorexia of infection can be adaptive depending on the organism and pathogen (Ayres and Schneider, 2009; Wang et al., 2016; Weis et al., 2017; Wang et al., 2018). We found that the effect of glucose supplementation on survival varies depending on the type of infection. In bacterial infection, glucose supplementation promotes mortality without impacting pathogen burden or inflammatory magnitude. This detrimental effect of glucose supplementation on bacterial infection is recapitulated without active pathogens by using LPS. The capacity for an organism to survive an infection requires both disease resistance, which coordinates pathogen clearance, and disease tolerance, which reflects the organism's ability to limit tissue damage and organ dysfunction caused by the infection (Ayres and Schneider, 2012; Medzhitov et al., 2012; Soares et al., 2014).

Sepsis is a life-threatening inflammatory syndrome due to dysregulated host response to an infection (Singer et al., 2016). Identifying metabolic pathways that participate in mechanisms of disease tolerance could lead to potential therapeutic targets to limit organ dysfunction and improve survival in sepsis. A major metabolic consequence of anorexia is a switch from fed to fasting metabolic pathways, including a shift from glucose metabolism to the utilization of alternative fuels. We found that glucose supplementation during LPS sepsis suppresses several core components of fasting metabolism, including fibroblast growth factor 21 (FGF21), an endocrine FGF hormone that mediates adaptive responses to metabolic stresses, including starvation (Fisher and Maratos-Flier, 2016).

FGF21 is a member of the endocrine FGF family that includes FGF15/19 and FGF23. FGF21 requires the coreceptor β -Klotho (KLB) for downstream ERK signaling via FGF receptors (Ogawa et al., 2007; Adams et al., 2012; Ding et al., 2012). FGF21 plays an important role in mediating adaptive responses to metabolic stresses. Basally, FGF21 is expressed in the liver,

¹Department of Internal Medicine (Nephrology) and Pharmacology, University of Texas Southwestern Medical Center, Dallas, TX; ²Department of Internal Medicine (Rheumatology), Yale University School of Medicine, New Haven, CT; ³Department of Immunobiology, Yale University School of Medicine, New Haven, CT; ⁴Department of Internal Medicine (Cardiology) and Molecular Biology, University of Texas Southwestern Medical Center, Dallas, TX; ⁵Howard Hughes Medical Institute, Chevy Chase, MD.

Correspondence to Sarah C. Huen: sarah.huen@utsouthwestern.edu; H.H. Luan's present address is NGM Biopharmaceuticals, South San Francisco, CA.

© 2021 Huen et al. This article is distributed under the terms of an Attribution–Noncommercial–Share Alike–No Mirror Sites license for the first six months after the publication date (see http://www.rupress.org/terms/). After six months it is available under a Creative Commons License (Attribution–Noncommercial–Share Alike 4.0 International license, as described at https://creativecommons.org/licenses/by-nc-sa/4.0/).





pancreas, and adipose tissue. Starvation increases hepatic FGF21 production, promoting ketogenesis and gluconeogenesis while inhibiting somatic growth (Potthoff et al., 2012). Overexpression of FGF21 in mice extends lifespan (Zhang et al., 2012) at the cost of female infertility and growth defects (Ding et al., 2012; Owen et al., 2013), suggesting that FGF21 functions as a trade-off in starvation adaptation to growth and reproduction.

As FGF21 functions as an adaptation hormone to metabolic stressors (Fisher and Maratos-Flier, 2016), we hypothesized that FGF21 may also act as a protective adaptation hormone to other challenges that lead to metabolic stress, such as infection and inflammation. We recently showed that circulating levels of FGF21 increase in mice injected with LPS (Wang et al., 2016), similar to what has been observed in septic patients (Gariani et al., 2013; Li et al., 2018; Ebrahimi et al., 2019). Fqf21-/- mice are more susceptible to death from endotoxemia, and treatment with FGF21 initiated after induction of bacterial inflammation can prolong their survival (Wang et al., 2016). Our findings suggest that increased FGF21 levels may represent an adaptive response that is critical for surviving other organismal challenges such as bacterial infections and could represent a novel therapeutic modality in bacterial sepsis. However, the origin of circulating FGF21 during bacterial inflammation and how FGF21 supports survival in bacterial infection are not well understood. Prior work suggested that the source of FGF21 during bacterial inflammation was not likely the liver and that the mechanism of FGF21 protection was due to ketone production (Feingold et al., 2012). However, we found that $Fgf21^{-/-}$ mice do not exhibit any defect in ketogenesis during LPS sepsis or have any significant differences in classic inflammatory markers (Wang et al., 2016). In this study, we investigated the tissue source and the effector function of circulating FGF21 during bacterial inflammation. Here, we show that during bacterial inflammation, circulating FGF21 is liver derived, is required for survival, and maintains thermoregulation and cardiovascular function.

Results and discussion

Circulating FGF21 during bacterial inflammation is hepatic in origin and required for survival

Given that treatment with recombinant FGF21 after LPS challenge can rescue FGF21-deficient mice from LPS-induced mortality (Wang et al., 2016), we examined whether constitutive overexpression of FGF21 could protect mice from LPS-associated mortality. Surprisingly, mice with transgenic overexpression of FGF21 driven by the liver-selective apolipoprotein E promoter (Fqf21-Tq; Inagaki et al., 2007) were not protected from endotoxemia and exhibited a trend toward increased mortality (Fig. 1 A). The lack of benefit of constitutively high levels of FGF21 suggests that regulated induction and timing of FGF21 activity may be critically important in promoting survival during endotoxemia. Indeed, we found that plasma FGF21 levels do not increase until later time points after LPS challenge (Fig. 1 B). Despite an early suppression, hepatic Fqf21 mRNA expression was induced to similar levels as fasting at later time points after LPS challenge, concurrent with the rise in plasma FGF21 (Fig. 1, C and D). We next explored the mechanism of hepatic Fgf21

expression in response to LPS. Regulation of FGF21 expression is context dependent. Several highly conserved metabolic and cellular stress response pathways, including peroxisome proliferator-activated receptor α (PPARα) and the integrated stress response, can lead to the expression of Fgf21. PPARa regulates hepatic Fqf21 transcription during fasting (Badman et al., 2007; Inagaki et al., 2007). Similar to fasting, the up-regulation of hepatic Fqf21 and increased circulating levels of FGF21 in response to LPS challenge are also PPARα dependent (Fig. 1, E-G). To determine whether the change in hepatic Fgf21 expression resulted in the increase in plasma FGF21 protein levels, we generated a mouse with hepatic-specific Fqf21 deletion (Alb-Cre; $Fgf21^{fl/fl}$, referred to as $Fgf21^{\Delta Liv}$, Fig. 1 H). $Fgf21^{\Delta Liv}$ mice failed to increase plasma FGF21 levels after LPS challenge, definitively proving that plasma FGF21 during bacterial inflammation is hepatic in origin (Fig. 1 I).

To determine the significance of hepatic FGF21 production during bacterial inflammation, we next investigated the effect of hepatic deletion of Fqf21 on the survival of mice during endotoxemia. Similar to Fqf21-/- mice (Wang et al., 2016), Fqf21^{ΔLiv} mice were also more susceptible to mortality from LPS (Fig. 1 J), suggesting that hepatic FGF21 production is required for survival. As LPS challenge models the sterile inflammation that accompanies bacterial infection, the increased mortality in FGF21-deficient mice in the absence of live bacteria suggests that FGF21 supports survival through promoting disease tolerance. To determine whether FGF21 contributes to disease resistance, we employed cecal ligation and puncture (CLP), a polybacterial infection model. While $Fgf21^{\Delta Li\nu}$ mice were more susceptible to mortality after CLP (Fig. 1 K), the bacterial load was no different between $Fqf21^{\Delta Li\nu}$ and WT controls (Fig. 1 L), suggesting that hepatic FGF21 confers protection against bacterial inflammation through promoting disease tolerance rather than bacterial clearance.

We next examined the effect of FGF21 deficiency on physiological and metabolic parameters in response to bacterial inflammation. FGF21 is known to promote thermogenesis in cold adaptation (Fisher et al., 2012; Ameka et al., 2019) and increase energy expenditure (Owen et al., 2014). Consistent with these known functions of FGF21, Fgf21^{ΔLiv} mice exhibited decreased body temperatures after CLP as well as high- and low-dose LPS challenge (Fig. 2 A). The suppressed body temperatures in Fqf21^{\Delta Liv} after LPS challenge are also associated with decreased energy expenditure and oxygen consumption (Fig. 2, B and C). FGF21 also plays a major role in glucose and lipid metabolism, interacting with several metabolic mediators, including adiponectin, glucocorticoids, and thyroid hormone (Potthoff et al., 2009; Holland et al., 2013; Domouzoglou et al., 2014; Liang et al., 2014; Patel et al., 2015). During bacterial sepsis, multiple metabolic changes occur, including dysglycemia, hyperlipidemia, dysthermia, and sick euthyroid syndrome (Van Wyngene et al., 2018). We reasoned that if FGF21 modulates metabolic pathways, it may limit metabolic derangement or support protective metabolic pathways in bacterial sepsis. However, we found no difference in blood glucose, free fatty acids, adiponectin, corticosterone, or thyroid hormone levels in LPS sepsis between WT and Fgf21^{-/-} mice (Fig. 2, D-G; and Fig. S1, A and B).



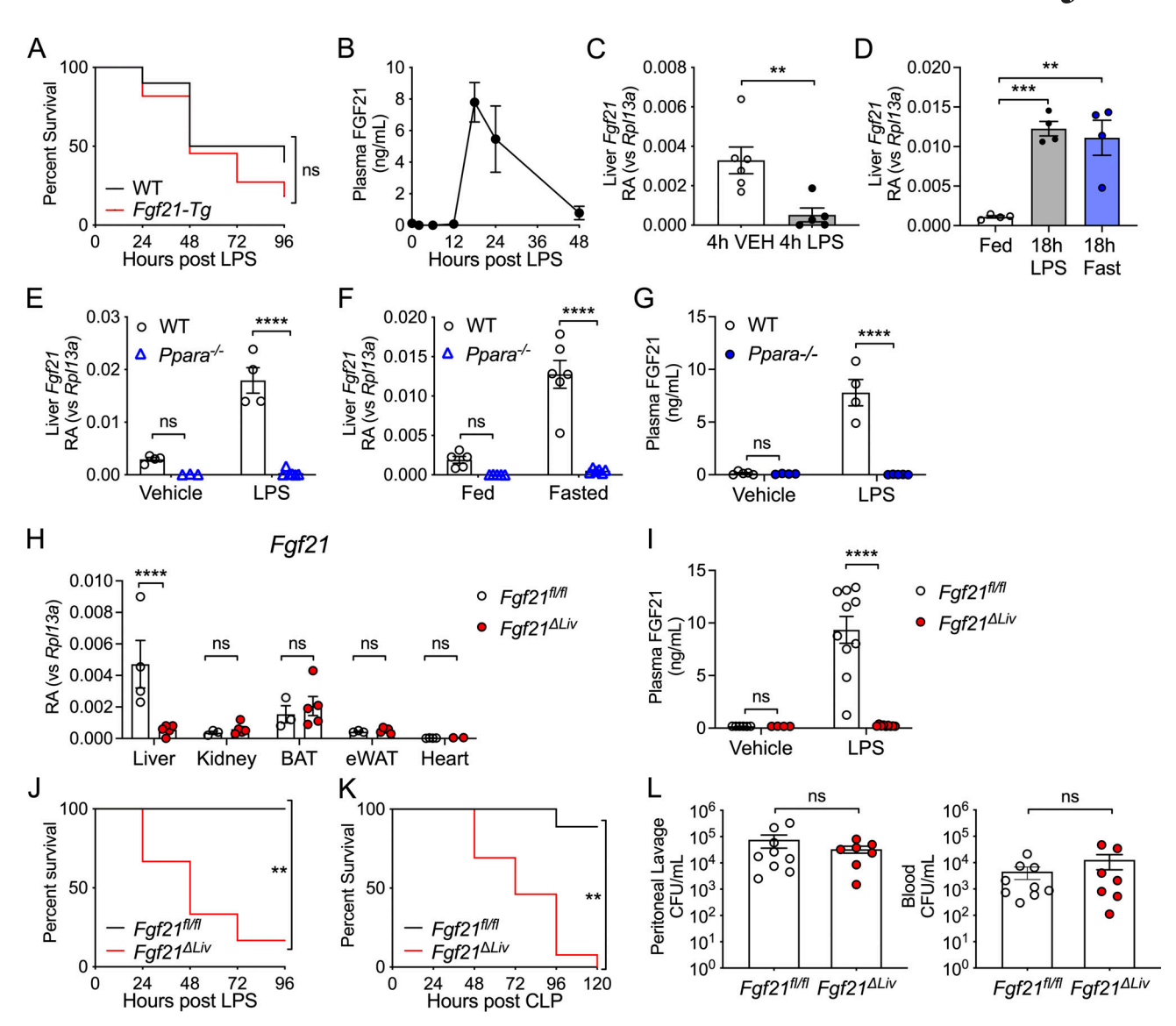


Figure 1. Increased circulating FGF21 during bacterial inflammation is hepatic in origin and required for survival. (A) Kaplan-Meier survival curve after 12.5 mg/kg i.p. LPS for WT and Fqf21-Tq mice. n = 10-11/group; pooled data from two independent experiments. (B) WT mice were challenged with 12.5 mg/kg i.p. LPS. Plasma FGF21 levels were measured by ELISA, n = 4–5/time point. Data are from one of two independent experiments with similar results. (c) Relative abundance (RA) of mRNA expression in whole-liver tissue 4 h after PBS vehicle (VEH) or 12.5. mg/kg i.p. LPS challenge in WT mice, shown relative to Rpl13a. n = 5-6/group; pooled data are from two of four independent experiments with similar results. (D) mRNA expression in whole-liver tissue, shown relative to Rpl13a, 18 h after PBS vehicle (Fed), 15 mg/kg i.p. LPS, or fasting in WT mice, n = 4/group; data are from one of six independent experiments with similar results. (E) mRNA expression of whole-liver tissue, shown relative to Rp[13a, 20 h after PBS vehicle or 15 mg/kg i.p. LPS in WT and Ppara^{-/-} mice. n = 3-7/group; data are from one of three independent experiments with similar results. (F) mRNA expression of whole-liver tissue, shown relative to Rpl13a, from ad libitum-fed or 24 h fasted WT and $Ppara^{-/-}$ mice. n = 5-6/group; data are from one of three independent experiments with similar results. (G) Plasma FGF21 levels by ELISA 18 h after PBS vehicle or 15 mg/kg i.p. LPS in WT and $Ppara^{-/-}$ mice. n = 4-5/group; data are from one of two independent experiments. **(H)** mRNA expression in whole tissue from $Fqf21^{fl/fl}$ and $Fqf21^{\Delta Liv}$ mice, shown relative to Rpl13a. n = 3-5/group; data are from one of two independent experiments. BAT, brown adipose tissue; eWAT, epididymal white adipose tissue. (I) Plasma FGF21 levels measured by ELISA 20 h after 5 mg/kg i.p. LPS or PBS vehicle in Fqf21^{fl/fl} and $Fgf(21^{\Delta Liv})$ mice. Vehicle n=4-6/group; LPS n=8-12/group; pooled data are from three independent experiments. (J) Kaplan-Meier survival curve after 10 mg/kg i.p. LPS for $Fgf21^{fl/fl}$ and $Fgf21^{\Delta Liv}$ mice. n = 5-6/group; data are from one of three independent experiments with similar results. (K) Kaplan–Meier survival curve after CLP for $Fqf21^{fl/fl}$ and $Fqf21^{\Delta Liv}$ mice. n = 9-13/group; pooled data are from two independent experiments. (L) CFUs cultured from mouse peritoneal lavage fluid and blood 24 h after CLP, n = 7-9/group; pooled data are from two independent experiments. **, P < 0.01; ***, P < 0.001; ****, P < 0.000, log-rank (Mantel-Cox) test (A, J, and K); two-sided, unpaired t test (C and L); one-way ANOVA with Dunnett's multiple comparisons test (D); two-way ANOVA with Sidak's multiple comparisons test (E-I). Data are expressed as mean \pm SEM.

We previously reported that the increased mortality in FGF21-deficient mice is not associated with increased inflammation (Wang et al., 2016). We next examined injury biomarkers of organs known to be susceptible to injury during

bacterial sepsis. Interestingly, we found that FGF21-deficient animals did not exhibit significant differences in hepatocyte injury (similar alanine aminotransferase activity and acute-phase response), cardiomyocyte injury (normal troponin levels), or



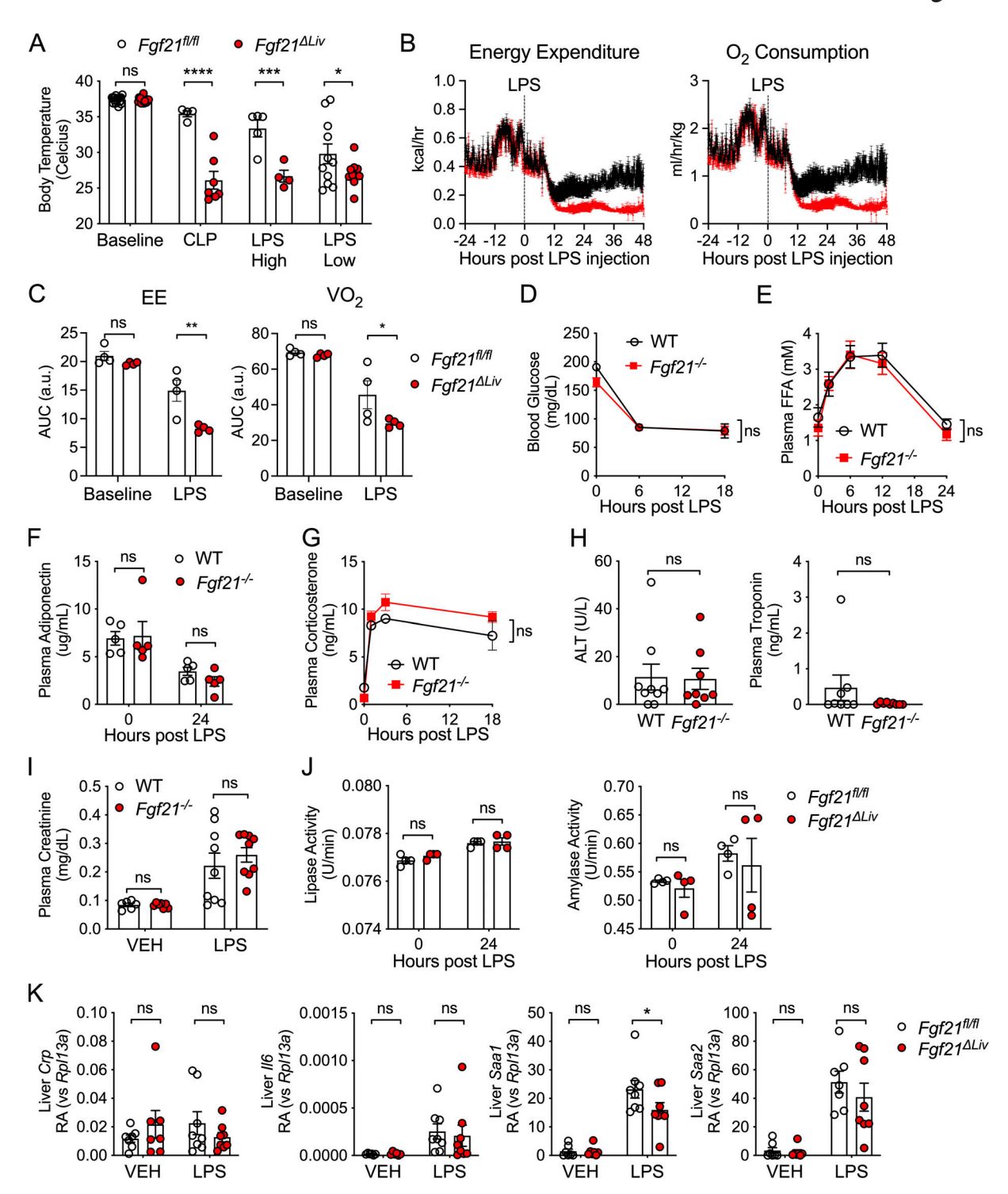


Figure 2. **FGF21 deficiency results in decreased body temperature after LPS challenge. (A)** Rectal temperatures of $Fgf21^{Il/fl}$ and $Fgf21^{\Delta Liv}$ mice 24 h after CLP, LPS high dose (10 mg/kg i.p.), and LPS low dose (5 mg/kg i.p.). n = 4-11/group; data are from one of two independent experiments (CLP, LPS high dose), and pooled data are from three independent experiments (LPS low). (B and C) Energy expenditure (EE) and oxygen consumption (VO₂) before and after 2.5 mg/kg i.p. LPS challenge in $Fgf21^{Il/fl}$ and $Fgf21^{\Delta Liv}$ mice. n = 4/group; data are from one of two independent experiments with similar results. **(C)** Area under the curve (AUC) from B. **(D-H)** WT and $Fgf21^{-l-}$ mice were challenged with 12.5 mg/kg i.p. LPS. **(D)** Blood glucose. n = 5/group; data are from one of four independent experiments with similar results. **(E)** Plasma free fatty acids (FFAs) by enzymatic assay. n = 5/group; data are from one of two independent experiments with similar results. **(F)** Plasma adiponectin measured by ELISA. n = 5/group; data are from one of two independent experiments with similar results. **(H)** Alanine aminotransaminase (ALT) activity measured by enzymatic activity assay and troponin measured by ELISA 24 h after LPS. n = 8-9/group; pooled data are from two independent experiments. **(I)** Plasma creatinine measured by HPLC 24 h after PBS vehicle (VEH) or 10 mg/kg i.p. LPS in WT and $Fgf21^{-l-}$ mice, n = 6-9/group; pooled data are from one of two independent experiments with similar results. **(K)** mRNA expression in whole-liver tissue 20 h after vehicle or 5 mg/kg i.p. challenge, shown relative to Rpl13a. n = 7-8/group; pooled data are from two independent experiments. Data are expressed as mean \pm SEM. *, P < 0.001; ****, P < 0.001; ****, P < 0.0001; *****, P < 0.0001; two-way ANOVA with Sidak's multiple comparisons test (A, C-G, and I-K) or unpaired two-sided t test (H).



kidney injury (similar creatinine levels) compared with WT controls during endotoxemia (Fig. 2, H, I, and K). Other known biomarkers for severity of illness in sepsis, including blood lactate, acidosis, and hypoxia, were measured and found to not significantly differ between WT and FGF21-deficient animals (Fig. S1, C and E). As FGF21 regulates pancreatic exocrine function and pharmacologic FGF21 can limit injury from pancreatitis (Coate et al., 2017; Hernandez et al., 2020), we next examined plasma amylase and lipase activity and found they were no different in FGF21-deficient mice (Fig. 2 J), suggesting that the protective effect of FGF21 in endotoxemia is unlikely to involve the pancreas. Thus, FGF21 mediates protection from endotoxemia through a mechanism that does not involve overt cellular damage.

KLB is required for survival in endotoxemia

As FGF21 signaling downstream of FGF receptors requires the coreceptor KLB (Ding et al., 2012), we next examined whether KLB is necessary for the protective effect of FGF21 in bacterial inflammation using whole-body Klb knockout (Klb-/-) mice. Indeed, we found that Klb-/- mice were more susceptible to mortality from endotoxemia and exhibited lower body temperatures after LPS challenge compared with heterozygous Klb+/littermate controls (Fig. 3, A and B). As FGF21-deficient and KLBdeficient animals are unable to maintain body temperature during endotoxemia, we next tested whether FGF21 was acting on the adipose tissue or centrally in the brain. To test the effect of FGF21 on adipose tissue, we generated mice with adiposespecific deletion of Klb (Adiponectin-Cre; Klb $^{fl/fl}$, Klb $^{\triangle Adipo}$). $Klb^{\Delta Adipo}$ mice had no difference in mortality after LPS, nor had any difference in body temperature compared with Klbfl/fl littermate controls (Fig. 3, C and D). While FGF21 may have a direct effect on adipose tissue for thermogenesis (Fisher et al., 2012), there are other nonadipose effects mediated via the central nervous system during acute cold exposure and pharmacologic dosing (Owen et al., 2014; BonDurant et al., 2017; Ameka et al., 2019). Many of the central effects of FGF21, including its effects on female reproduction, circadian behavior, metabolism, thirst response to ketogenic diet and alcohol, sweet and alcohol preference, and food choice during protein restriction, have been reported to act via KLB expression in CamK2A-expressing neurons, mainly in the suprachiasmatic nucleus (SCN) of the hypothalamus, in studies using the Camk2a-Cre;Klbfl/fl mouse model (Klb^{\Delta Camk2a}; Bookout et al., 2013; Owen et al., 2013; Owen et al., 2014; Talukdar et al., 2016; Song et al., 2018; Hill et al., 2019). Surprisingly, $Klb^{\Delta Camk2a}$ mice exhibited no difference in body temperature or mortality in response to LPS challenge compared with Klbfl/fl littermate control mice (Fig. 3, E and F). While liver KLB expression is high, downstream FGF receptor signaling via KLB in the liver is thought to be primarily activated by FGF15 (human orthologue FGF19) due to its preferential affinity for FGFR4, which is expressed in the liver (Kurosu et al., 2007). As it is unclear whether in other contexts, such as bacterial sepsis, FGF21 could signal via liver KLB, we generated animals with hepatic-specific deletion of Klb (Alb-Cre;Klb^{fl/fl}, $Klb^{\Delta Li\nu}$). $Klb^{\Delta Li\nu}$ mice also had similar survival and body temperature in response to LPS compared with their WT Klbfl/fl littermates (Fig. 3, G and H). These data suggest that in bacterial

sepsis, KLB is required for survival; however, the mechanism by which FGF21 acts to promote survival is either independent of the well-described FGF21 target tissues of the brain, adipose, and liver or involves FGF21 signaling on multiple KLB-expressing tissues.

FGF21 deficiency results in decreased body temperature and heart rate in LPS endotoxemia

Sepsis physiology is characterized by hemodynamic instability driven by reduced systemic vascular resistance and cardiac dysfunction, which leads to shock and organ dysfunction (Drosatos et al., 2015). As a result of shunting of blood and decreased cardiac output, low body temperature could be reflective of severe heart failure (Casscells et al., 2005). As recent studies of cardiomyopathy and cardiac ischemia suggest that FGF21 can act on the heart to limit cardiac injury (Planavila et al., 2013; Patel et al., 2014), we considered the possibility that FGF21 may affect cardiac function during bacterial sepsis. Fqf21^{\Delta Liv} and littermate control mice underwent echocardiograms at baseline and again 18 h after LPS challenge, when plasma FGF21 peaks (Fig. 1 B). Despite normal troponin levels, Fgf21^{△Liv} mice have decreased heart rate and cardiac contractility (Fig. 4, A-C). As pharmacologic dosing of FGF21 has been reported to increase blood pressure (Kim et al., 2017; Turner et al., 2018), we next asked whether FGF21 has an effect on blood pressure during bacterial sepsis. Ambulatory telemetry confirmed the decreased heart rate in Fgf21^{ΔLiv} mice after LPS observed by echocardiography; however, there was no significant difference in blood pressure (Figs. 4 D and S2 A), suggesting that the decrease in ejection fraction is primarily reflecting the decrease in heart rate. Treatment with recombinant FGF21 in Fqf21^{ΔLiv} mice increased body temperature and heart rate, although the difference in heart rate did not reach statistical significance (Fig. 4, E-G). FGF21 deficiency had no overt effect on markers of cardiac inflammation, fatty acid oxidation, acute stress response pathways, and cardiac cell apoptosis after LPS challenge (Fig. S3, A-D). While heart failure often results in relative tachycardia, decreased blood pressure, and end-organ damage due to decrease perfusion, $Fqf2l^{\Delta Li\nu}$ mice were able to preserve their blood pressure with the lack of other end-organ damage (lack of difference in liver and kidney injury biomarkers) suggesting the possibility of a primary autonomic defect resulting in a bradyarrhythmia increasing the risk of sudden cardiac death (Vaseghi and Shivkumar, 2008). Moreover, the absence of elevated troponin levels and other direct cardiac damage-related biomarkers in FGF21-deficient animals suggests an indirect effect on the heart.

To explore whether FGF21 acts directly or indirectly on the heart, we next determined whether there is direct FGF21 signaling in the heart. Prior reports suggest that KLB is expressed in the heart (Liu et al., 2013; Planavila et al., 2013; Patel et al., 2014). However, we found that relative to other tissues, Klb expression in the heart is extremely low and is further decreased after LPS challenge (Fig. 4 H). Acute treatment with FGF21 did not activate ERK signaling in the heart (Fig. 4 I), further supporting an indirect effect of FGF21 on the heart. Instead, we found ERK signaling in the aorta and the hindbrain (Fig. 4 I).



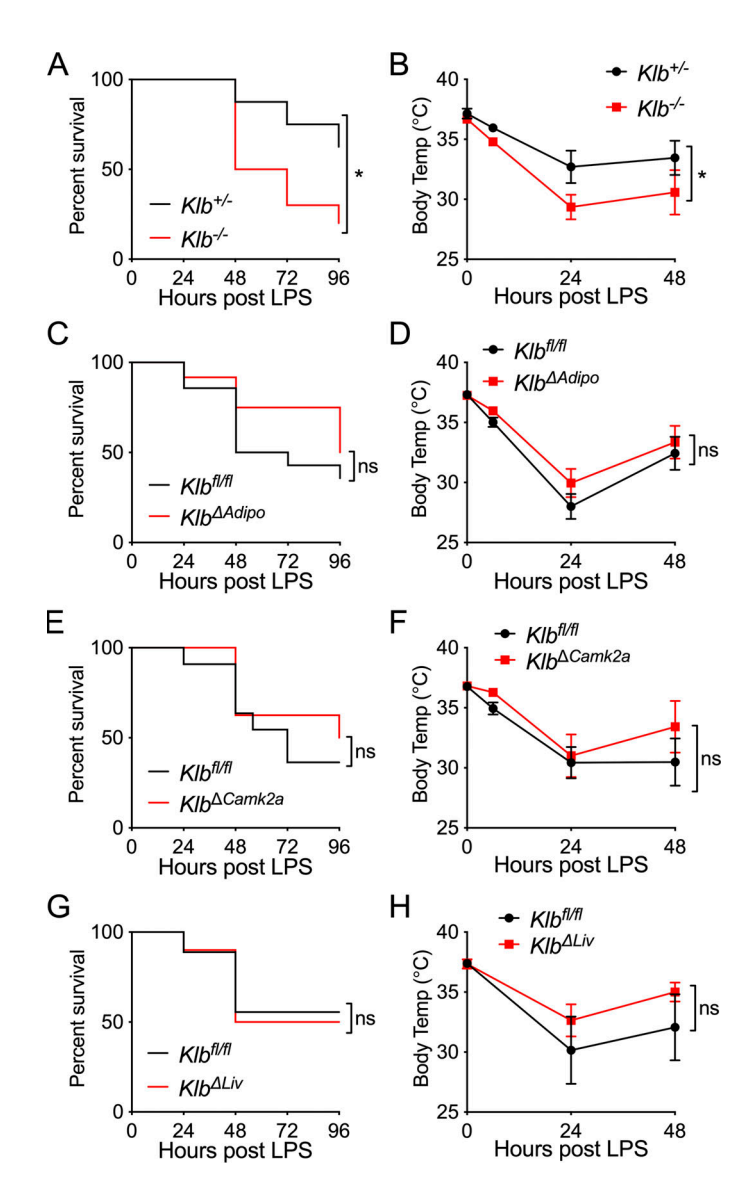


Figure 3. **KLB signaling is required for surviving endotoxemia.** (**A** and **B**) $Klb^{+/-}$ and $Klb^{-/-}$ mice were challenged with 10 mg/kg i.p. LPS, n = 8-10/group; data are from one of three independent experiments with similar results. (**A**) Kaplan–Meier survival curve. (**B**) Rectal temperatures. (**C** and **D**) $Klb^{fl/fl}$ and $Klb^{\Delta Adipo}$ mice were challenged with 15 mg/kg i.p. LPS, n = 10-14/group; pooled data are from two independent experiments. (**C**) Kaplan–Meier survival curve. (**D**) Rectal temperatures. (**E and F**) $Klb^{fl/fl}$ and $Camk2a-Cre;Klb^{fl/fl}$ ($Klb^{\Delta Camk2a}$) mice were challenged with 15 mg/kg i.p. LPS, n = 8-11/group; pooled data are from two independent experiments. (**E**) Kaplan–Meier survival curve. (**F**) Rectal temperatures. (**G and H**) $Klb^{fl/fl}$ and $Alb-Cre;Klb^{fl/fl}$ ($Klb^{\Delta Liv}$) mice were challenged with 10 mg/kg i.p. LPS, n = 9-10/group; pooled data are from two independent experiments. (**G**) Kaplan–Meier survival curve. (**H**) Rectal temperatures. Data are expressed as mean \pm SEM. *, P < 0.05; log-rank (Mantel–Cox) test (A, C, E, and G) or two-way ANOVA with Sidak's multiple comparisons test (B, D, F, and H).

Using a KLB-TdTomato (Klb^{TdTm}) reporter mouse (Coate et al., 2017), we found KLB expression in the aorta by Western blot. Similar to prior reports of in situ hybridization of Klb in the brain (Bookout et al., 2013), we found KLB-expressing cells in the area postrema (AP) and the nucleus of the solitary tract (NTS; Fig. 4, J and K). Moreover, ERK activation in KLB-expressing cells in the AP was observed following acute FGF21 treatment (Fig. 4 J). Consistent with a lack of phenotype in the $Klb^{\Delta Camk2a}$ mice in which Klb is deleted from the SCN, we found that cFos, a marker of neuron activation, colocalized with KLB more in the AP than the NTS, but not with KLB-expressing cells in the SCN after LPS challenge (Fig. 4 K). Moreover, the $Klb^{\Delta Camk2a}$ mouse model does not effectively delete Klb in the hindbrain (Bookout et al., 2013).

These data collectively suggest that hepatic FGF21 promotes survival during bacterial inflammation by maintaining body temperature and heart rate independent of FGF21 signaling in the forebrain, hypothalamus, and the adipose tissue, which are operative in adaptation to cold and caloric deprivation. The mechanism by which FGF21 acts during bacterial sepsis may involve direct FGF21 action on multiple tissues, or it may involve an alternative FGF21 target tissue, including the endothelium, which can control systemic vascular tone and contribute to cardiac function via endothelial factors (Premer et al., 2019), and regions of the hindbrain, the AP and NTS, known to regulate autonomic control of physiological systems, including the cardiovascular system (Price et al., 2008; Coote and Spyer, 2018).



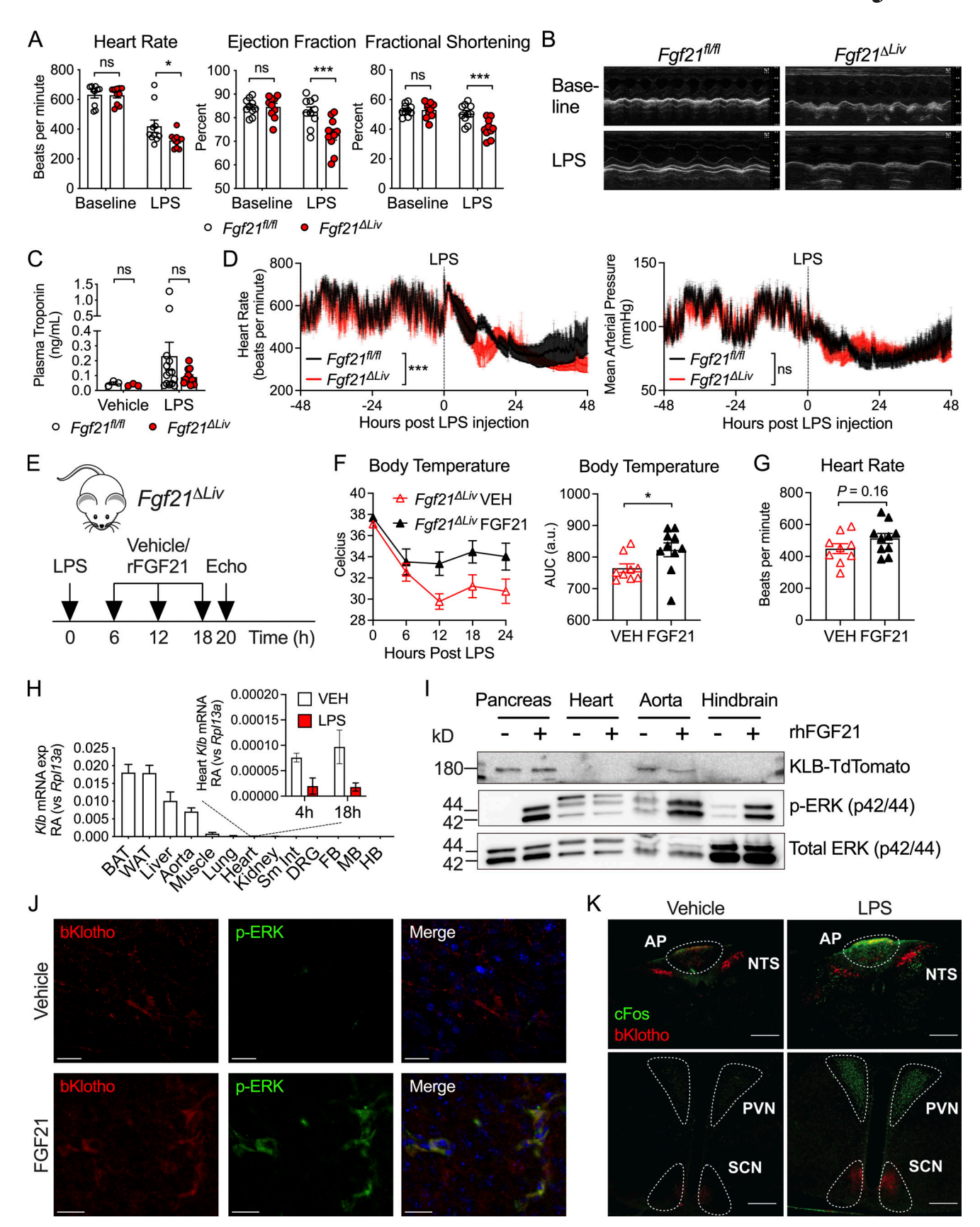


Figure 4. **FGF21 deficiency causes bradycardia during LPS endotoxemia.** (A and B) Echocardiography performed on $Fgf21^{fl/fl}$ and $Fgf21^{\Delta Liv}$ mice before (baseline) and 18 h after 5 mg/kg i.p. LPS. n = 10/group; pooled data are from three independent experiments. (B) Representative echocardiogram windows. (C) Plasma troponin in $Fgf21^{fl/fl}$ and $Fgf21^{\Delta Liv}$ mice 20 h after PBS vehicle or 5 mg/kg i.p. LPS. Vehicle n = 3/group; LPS n = 10-12/group; pooled data are from three



independent experiments. (D) Ambulatory blood pressure and heart rate of $Fqf21^{fl/fl}$ and $Fqf21^{\Delta Liv}$ mice measured by in vivo telemetry before and after 2 mg/kg i.p. LPS. n = 4/group; pooled data are from three independent experiments. Mean arterial pressure and heart rate measured every minute and shown as mean ± SEM within each group. (E-G) Fqf21^{ΔLiv} mice were challenged with LPS 5 mg/kg i.p. Recombinant mouse FGF21 10 ng i.v. or PBS vehicle was administered starting at 6 h after LPS and then every 6 h for three doses. n = 9-10/group; pooled data are from two independent experiments. Experimental workflow shown in E. (F) Rectal temperatures and areas under the curve (AUC). (G) Heart rate by echocardiography was performed at 20 h after LPS injection. (H) Klb mRNA expression in whole tissue from WT mice, shown relative to Rpl13a; inset shows RA of heart Klb after PBS vehicle or LPS treatment. n = 3-4/group; results of one of two independent experiments with similar results are shown. qPCR Ct values are as follows: brown adipose tissue (BAT), 22; white adipose tissue (WAT), 22; liver, 23; aorta, 25; heart, 30 at baseline, 32 after LPS. FB, forebrain; MB, midbrain; HB, hindbrain; Sm Int, small intestine; DRG, dorsal root ganglia. (1) Whole-tissue protein lysates from Klb^{TdTm} mice immunoblotted for RFP (to detect KLB-TdTomato), p-ERK, and total ERK 10 min after 1 mg/kg i.p. recombinant human FGF21 (rhFGF21). The hindbrain region, including AP and NTS, was grossly dissected. Pancreas tissue was included as a positive control. Representative blots from one of three independent experiments are shown. (1) Brains from KlbTdTm mice were harvested 10 min after 1 mg/kg i.p. rhFGF21 treatment. 50-micron fixed brain vibratomed sections were immunostained for RFP and p-ERK. Representative images of the AP from one of two independent experiments are shown. Scale bars represent 20 µm. (K) Brains from Klb^{TdTm} mice were harvested 18 h after 15 mg/kg i.p. LPS or PBS vehicle. 50-micron fixed brain vibratomed sections were immunostained for RFP and cFos. Representative images from one of three independent experiments are shown. PVN, paraventricular nucleus. Scale bars represent 200 µm. *, P < 0.05; ***, P < 0.001; two-way ANOVA with Sidak's multiple comparisons test (A and C), two-way ANOVA (D), or unpaired two-sided t test (F and G). Data are expressed as mean \pm SEM.

Studies of decerebrate rats suggest that the hindbrain can also contribute to both thermogenesis and heart rate control independent of the forebrain and the hypothalamus (Hermann et al., 2006; Nautiyal et al., 2008). The coupling of heart rate and body temperature phenotypes in FGF21-deficient mice is therefore of interest due to the presence of LPS-activated KLB-expressing cells in the hindbrain. Moreover, activation of the cholinergic nervous system, including the AP and NTS regions, has been described in rodent models of sepsis and is associated with bradycardia and a significant decrease in heart rate variability (HRV), a measure of sympathovagal balance (Fairchild et al., 2009; Fairchild et al., 2011). Consistent with these published studies, we also found that both $Fgf21^{fl/fl}$ and $Fgf21^{\Delta Li\nu}$ mice exhibit a decrease in HRV (Fig. S2, B and C). However, compared with WT animals, FGF21-deficient mice exhibit more bradycardia and increased HRV. While this observation appears to be inconsistent with clinical data that suggest that decreased HRV associates with poor prognostic indicator of sepsis (Ahmad et al., 2009), rodent models of acute bacterial infection with continuous electrocardiography suggest a more complex relationship between risk of mortality and HRV. While nonsurviving mice had lower HRV overall compared with survivors, nonsurviving mice also exhibited periods of increased HRV and bradycardia before death (Fairchild et al., 2011).

Limitations, caveats, and open questions

Further research is needed to determine whether KLB-expressing regions in the AP and NTS participate in coordinating FGF21-mediated thermogenic and compensatory cardiac responses to bacterial inflammation. One compelling hypothesis based on our data is that the hypothermia, excessive bradycardia, and periods of increased HRV observed in FGF21-deficient mice may reflect an imbalance of parasympathetic and sympathetic activity resulting from abnormal signaling in the hind-brain. One limitation of our study is that the in vivo telemetry devices used in our studies are unable to report electrocardiography. Therefore, determination of heart rhythm and standard measurement of HRV by R-R interval were not possible. We did not observe any differences in respiratory rate, oxygenation, or ventilation after LPS challenge between FGF21-deficient and WT animals (Fig. S1, D and E). However, the lack of differences

in respiration does not rule out altered autonomic outflow, as our measurement method via pulse oximetry may not be sensitive enough to detect a difference in respiratory rate (Grimaud and Murthy, 2018) and HRV is considered the best-available index to estimate sympathovagal balance (Goldberger, 1999). Future studies targeting KLB-expressing neurons in the hindbrain with more accurate and precise continuous measurements of temperature, electrocardiographic waveforms, HRV, and respiratory rate are needed.

In summary, we have identified hepatic FGF21 as a thermogenic and chronotropic factor acting independent of the forebrain and hypothalamus in bacterial inflammation. The regulation of hepatic FGF21 expression in endotoxemia is PPARa dependent as it is in fasting. A growing body of evidence (Wang et al., 2016; Rao et al., 2017; Weis et al., 2017) supports the concept that in response to specific challenges, certain physiological responses that have often been considered maladaptive, such as anorexia of acute illness or metabolic derangements of sepsis, are in fact coordinated defense mechanisms to promote survival and tissue protection. Our study further supports the concept that metabolic reprogramming through endocrine factors, such as FGF21, is a critical component of disease tolerance. Sepsis remains a deadly condition lacking therapeutic options. FGF21 may represent a promising therapeutic target; however, further research in understanding its dynamic expression and mechanism of action is needed.

Materials and methods

Mice

All animal experiments were performed in accordance with institutional regulations after protocol review and approval by Institutional Animal Care and Use Committees at Yale University and University of Texas (UT) Southwestern Medical Center. Fgf21^{-/-} (Potthoff et al., 2009), Fgf21^{ΔLiv} (generated from Fgf21^{fl/fl} [Potthoff et al., 2009] and Alb-Cre from The Jackson Laboratory; stock 003574), Fgf21-Tg (Inagaki et al., 2007), Klb^{-/-} (Ding et al., 2012), Klb^{TdTm} (Coate et al., 2017), Klb^{ΔAdipo} (Lan et al., 2017), and Klb^{ΔCamk2a} mice (Bookout et al., 2013) were generous gifts from Drs. David J. Mangelsdorf (University of Texas Southwestern Medical Center, Dallas, TX) and Steve Kliewer (University of



Texas Southwestern Medical Center, Dallas, TX). C57BL/6J (stock 000664) and $Ppara^{-/-}$ ($Ppara^{tmlGonz}$ /J, stock 008154) mice were purchased from The Jackson Laboratory. $Klb^{-/-}$ mice were maintained on a mixed (129Sv/C57BL/6) background, as $Fgf15^{-/-}$ and $Klb^{-/-}$ mice are embryonic lethal on a pure C57BL/6 background (Kong et al., 2014). All other mouse strains were maintained on a C57BL/6 background.

For the LPS endotoxemia, mice were injected i.p. with the indicated dose of LPS derived from *Escherichia coli* 055:B5 (Sigma-Aldrich) diluted in 100 μ l PBS. LPS dosing varies across experiments due to mouse strain and LPS batch/lot differences. An ~50% lethal dose of LPS is determined empirically for each mouse strain and LPS batch. Core body temperature was measured by rectal probe thermometry (Physitemp TH-5 Thermalert).

CLP was performed similar to standard protocols (Toscano et al., 2011). Briefly, mice were anesthetized with a ketamine/ xylazine (120 mg/kg; 16 mg/kg) mixture and given perioperative and postoperative buprenorphine (0.1 mg/kg) for analgesia. An ∼1-cm midline laparotomy was performed, and the cecum was exposed. The cecum was ligated with 4−0 silk suture (Ethicon) 1 cm from the tip of the cecum and perforated through and through with a 25-gauge needle. The cecum was gently squeezed to extrude a small amount of fecal contents and returned back into the peritoneum. The peritoneal wall was closed using 4−0 chromic gut (CP Medical). The skin was closed with surgical glue and staples. Mice were given 1 ml sterile saline subcutaneously and temporarily placed on a heating pad to aid in recovery.

Recombinant FGF21 (R&D Systems) was used for FGF21 rescue and signaling experiments. For recombinant FGF21 rescue experiments, FGF21 supplementation was done by retro-orbital injection of 10 ng recombinant mouse FGF21 in 100 µl PBS per injection starting at 6 h after LPS injection and administered every 6 h for three doses. For acute FGF21 signaling experiments, an i.p. injection of recombinant human FGF21 (1 mg/kg i.p.) was used.

Quantification of bacterial load

Bacterial titers of peritoneal lavage fluid and blood from mice 24 h after CLP were determined as previously described (Medina, 2010). Briefly, peritoneal lavage fluid (5 ml sterile PBS) and blood were serially diluted, plated on blood agar (tryptone soya agar with 5% sheep blood) plates (Thermo Fisher Scientific), and incubated at 37°C for 18 h.

Plasma cytokine, metabolite, and tissue injury marker analysis

Blood glucose was determined by whole blood obtained by tail vein prick and measured using a glucometer (OneTouch). For other tests, whole blood was harvested from mice by retroorbital bleeding, and plasma was isolated using lithium heparin coated plasma separator tubes (BD). Plasma Troponin-I concentration (Life Diagnostics), alanine aminotransferase activity (Cayman Chemical), Adiponectin (Abcam), nonesterified free fatty acids (Wako Diagnostics), FGF21 (R&D Systems and BioVendor), corticosterone (Enzo), thyroid-stimulating hormone, free T4 (LSBio), and lipase and amylase activity (Sigma-Aldrich) were assayed using kits according to manufacturers' protocols. Venous blood gas

and lactate levels were measured using the i-STAT1 Handheld Analyzer (Abaxis; cartridges CG4+ and CG8+). Plasma creatinine was assayed using HPLC at the George M. O'Brien Kidney Center at Vala

Metabolic chamber

Energy expenditure and oxygen consumption after LPS challenge was measured by indirect calorimetry using metabolic cages (Sable Systems International; Promethion). A 2-d period of acclimation was followed by 2 d of steady-state recording before experimentation. After 2 d of baseline recordings, LPS was administered i.p., and mice were returned to the metabolic chambers. Recordings were continued for another 48 h after LPS challenge.

Cell culture

To generate positive controls for caspase-3 Western blots, Hepal-6 cells (ATCC; CRL-1830) were maintained in DMEM (Corning; 10–013-CV) with 10% FBS (VWR) and 1% penicillinstreptomycin (Sigma-Aldrich). Staurosporine (Cayman Chemical) was administered at 5 μ M for up to 24 h.

RNA extraction and quantification

For tissue RNA extraction, tissues were harvested into RNA Bee RNA isolation reagent (Tel Test) and disrupted by bead homogenization in Lysing Matrix D tubes using a FastPrep-24 5G homogenizer (MP Biomedicals) or in Fisherbrand Pre-Filled Bead Mill Tubes using a Fisherbrand Bead Mill 24 Homogenizer (Fisher Scientific). RNA was extracted using the RNeasy or Direct-Zol Kits according to manufacturer's protocol (Qiagen or Zymo Research, respectively). cDNA synthesis was performed using Moloney murine leukemia virus reverse transcription (Clontech) with oligo(dT) primers. Quantitative RT-PCR (qRT-PCR) reactions were performed on either a CFX96/CFX384 Real-Time System (Bio-Rad) or QuantStudio 7 Flex (Applied Biosystems) using PerfeCTa SYBR Green SuperMix (Quanta Biosciences) or iTaqTM Universal SYBR Green Supermix (Bio-Rad), and transcript levels were normalized to Rpl13a. Primers used for qRT-PCR are cataloged in Table 1.

Western blot

Tissue samples were harvested and snap frozen in liquid nitrogen. Frozen tissues were bead homogenized in RIPA buffer (Teknova) supplemented with the Halt protease and phosphatase inhibitor cocktail (Thermo Fisher Scientific), according to the manufacturer's protocols. Equal amounts of protein were loaded per well (Bio-Rad). Protein was transferred onto activated polyvinylidene fluoride membrane (Bio-Rad) and then blocked in 5% milk in TBST (20 mM Tris, 150 mM NaCl, and 0.05% Tween 20) for 30 min. Membranes were incubated with primary antibodies overnight at 4°C. Primary antibodies used include anti-RFP (Rockland; 600401379), p-ERK (Cell Signaling Technology [CST]: 4370), total ERK (CST: 4695), and caspase-3 (CST; 9662). Membranes were washed three times with TBST and then incubated with secondary antibodies for 1 h at room temperature. After washing, protein was visualized using enhanced chemiluminescence reagent (Bio-Rad).



Table 1. Primers used for qRT-PCR

Gene	Forward primer	Reverse primer
Becn1	5'-CCCCAGGCAGCATTGATTTC-3'	5'-AGCAGCTGGAGTTGGATGAC-3'
Bnip3	5'-TCGACTTGACCAATCCCATATCC-3'	5'-TCCCAGACACCACAAGATACC-3'
Cat	5'-TTCAGTGACCGAGGGATTCC-3'	5'-TTCCTGAGCAAGCCTTCCTG-3'
Ccl2	5'-AGGTGTCCCAAAGAAGCTGT-3'	5'-ACAGAAGTGCTTGAGGTGGT-3'
Cd36	5'-ACACACCACCATTTCTTCTC-3'	5'-GCTCCTTGGCATGGTAGAGA-3'
Cpt1a	5'-TTATGTGAGTGACTGGTGGGAGG-3'	5'-ATGGGTTGGGGTGATGTAGAGC-3'
Cpt1b	5'-AGGCTCCAGGGTTCAGAAAG-3'	5'-AACATGTACCGCCTAGCCAT-3'
Сгр	5'-AGCTTCTCGGACTTTTGGT-3'	5'-AATCGTACTTCAGCACCACCC-3'
Ddit3	5'-TCTCATCCCCAGGAAACGAAG-3'	5'-TGTGCGTGTGACCTCTGTTGG-3'
Edn	5'-CCAAGGAGCTCCAGAAACAG-3'	5'-GGTGAGCGCACTGACATCTA-3'
Fgf21	5'-CCTCTAGGTTTCTTTGCCAACAG-3'	5'-AAGCTGCAGGCCTCAGGAT-3'
Hmox1	5'-CATCCAAGCCGAGAATGCTG-3'	5'-CCTCAGGGAAGTAGAGTGGGG-3'
Il1a	5'-ACCCGACTTTGTTCTTTGGTG-3'	5'-GAGAAGACCAGCCCGTGTTG-3'
Il1b	5'-CAGTTGTCTAATGGGAACGTCA-3'	5'-GCACCTTCTTTTCCTTCATCTTT-3'
Il6	5'-GACTTCCATCCAGTTGCCTTCTTGG-3'	5'-CCAGTTTGGTAGCATCCATCATTTCT-3'
Il17a	5'-ACTACCTCAACCGTTCCACG-3'	5'-TTCCCTCCGCATTGACACAG-3'
Il17f	5'-ACGTGAATTCCAGAACCGCT-3'	5'-TGATGCAGCCTGAGTGTCTG-3'
Il18	5'-GACAAAGAAAGCCGCCTCAA-3'	5'-TCATTTCCTTGAAGTTGACGCA-3'
Klb	5'-GATGAAGAATTTCCTAAACCAGGTT-3'	5'-AACCAAACACGCGGATTTC-3'
Nos2	5'-GAATCTTGGAGCGAGTTGTGG-3'	5'-CAGGAAGTAGGTGAGGGCTTG-3'
Pdk4	5'-TGCCTGACCGCTTAGTGAACAC-3'	5'-CTTGAGCCATTGTAGGGACCAC-3'
Ppargc1a	5'-GTAAATCTGCGGGATGATGG-3'	5'-GGGTCAAAATCGTCTGAGTTG-3'
Rpl13a	5'-GAGGTCGGGTGGAAGTACCA-3'	5'-TGCATCTTGGCCTTTTCCTT-3'
Saa1	5'-CTGACATGAAGGAAGCTAACTGGA-3'	5'-GCCGAAGAATTCCTGAAAGGC-3'
Saa2	5'-AGGAAGCTGGCTGGAAAGAT-3'	5'-CAGTATTTGGCAGGCAGTCC-3'
Sod2	5'-CAGCCTGAACCTTGGACTCC-3'	5'-ACAACTCAGGTCGCTCTTCAG-3'
Tgfb1	5'-TGAGTGGCTGTCTTTTGACG-3'	5'-GGTTCATGTCATGGATGGTG-3'
Tnfa	5'-TCTGTCTACTGAACTTCGGGGTG-3'	5'-ACTTGGTGGTTTGCTACGACG-3'
Ucp2	5'-TGCACTCCTGTGTTCTCCTG-3'	5'-GGGACCTTCAATCGGCAAGA-3'
Ulk1	5'-TTGACTCGGATGTTGCTGGG-3'	5'-GTGGAGACCTGGCTGACTAC-3'

Cardiorespiratory measurements

Transthoracic echocardiography was recorded in awake mice using VisualSonics Vevo 2100 small-animal echocardiography machine. Views were taken in planes that approximated the parasternal short-axis view in humans. Ejection fractional shortening, and heart rate were obtained from M-mode parasternal short-axis measurements. Ultrasound images were recorded and analyzed by an experienced technologist with expertise in mouse ultrasound imaging. The technologist was blind to the treatments and genotypes of the mice in this study.

Breath rate and blood oxygen saturation were measured by pulse oximetry using the MouseOx Plus (Starr Life Sciences).

Ambulatory continuous blood pressure and heart rate measurements were performed by the Animal Physiology and Phenotyping Core within the George M. O'Brien Kidney Center at Yale. Briefly, a blood pressure transducer (DSI; TA11-PA-C10)

was surgically implanted under anesthesia into one carotid artery. Mice were allowed to recover for 7 d before recording of baseline values and then given 2 mg/kg i.p. LPS. Measurements were recorded every minute.

Immunostaining of mouse tissues

Brains from *Klb*^{TdTm} mice were harvested 18 h after 15 mg/kg i.p. LPS or PBS vehicle and fixed in 10% neutral buffered formalin overnight. Fixed brains were then vibratomed (50-micron sections). Brain sections were immunostained for RFP (Rockland; 600401379), cFos (Santa-Cruz Biotechnology; C-10, sc-271243), and phospho-p44/42 MAPK (CST; 9106, Erk1/2, Thr202/Tyr204) antibodies. Images of immunostained sections were acquired using the Axio Scan.Z1 (Zeiss) and LSM 880 confocal microscope (Zeiss). Images were processed using Zen 2.3, Blue Edition (Zeiss).



Hearts were harvested and fixed in 10% neutral buffered formalin overnight. Hearts were embedded in paraffin and sectioned in the 4-chamber view by the UT Southwestern Histo Pathology Core. Terminal dUTP nick-end labeling (TUNEL) staining of the heart sections was performed using the CardioTACS In Situ Apoptosis Detection Kit (R&D Systems) following manufacturer's instructions. For TUNEL staining quantification for each individual mouse heart, 20 random nonoverlapping fields per ventricle and 10 random nonoverlapping fields per atria were taken at 400× magnification on a Nikon Eclipse 80i microscope using a Nikon DS-Fi3 camera by an investigator blinded to the experimental manipulation. The total number of Nuclear Fast Red-positive cells and TACS Blue (TUNEL)-positive cells per high-power field were quantified using Image] to generate a final percent TUNEL-positive count. Due to the low frequency of TACS Blue (TUNEL)-positive cells, validation of TUNEL-positive cells was done manually by a blinded investigator. Positive (TACS-nuclease-treated sections) and unlabeled (terminal deoxynucleotidyl transferase enzyme omitted) controls were used to confirm TUNEL-positive and background TACS Blue labeling, respectively.

Statistics

Statistical information is indicated in figure legends. Statistical analyses were performed using Prism 8.0 (GraphPad Software). Where appropriate, Student's *t* test or ANOVA (one or two way) with multiple comparison analysis (Dunnett's or Sidak's, respectively) was used. Kaplan–Meier survival curves were compared using log-rank Mantel–Cox test. A P value < 0.05 was considered statistically significant.

Online supplemental material

Fig. S1 supplements Fig. 2 and shows sepsis biomarkers that do not differ between WT and FGF21-deficient mice. Fig. S2 supplements Fig. 4 D and shows the hourly averages of the differences in heart rate and blood pressure as well as the minute-to-minute HRV after LPS challenge. Fig. S3 shows the lack of evidence of a direct FGF21 effect on the heart during endotoxemia, as FGF21 deficiency did not result in any differences in cardiac markers of inflammation, fatty acid oxidation, acute stress response, or cell apoptosis.

Acknowledgments

We thank members of the Medzhitov and the Mangelsdorf/ Kliewer laboratories for helpful discussions and David Mangelsdorf and Steven Kliewer for making available the mouse models used in this study.

This study was supported by the Howard Hughes Medical Institute, Else Kröner Fresenius Foundation, the Blavatnik Family Foundation, and the National Institutes of Health (grants AI046688, AI089771, and CA157461). S.C. Huen was supported by the National Institutes of Health (grants K08DK110424 and R35GM137984) and the American Society of Nephrology Carl W. Gottschalk Research Scholar Grant. A. Wang was supported by the National Institutes of Health (grants T32 AR07107-39 and K08AI128745). Plasma creatinine samples and invasive

hemodynamic telemetric monitoring were performed through the George M. O'Brien Kidney Center at Yale (National Institutes of Health grant P30-DK079310). Preparation of the heart histology sections were processed by the UT Southwestern Histo Pathology Core via the George M. O'Brien Kidney Research Core Center at UT Southwestern Medical Center (National Institutes of Health grant P30-DK079328).

Author contributions: S.C. Huen, A. Wang, and R. Medzhitov designed the research studies and analyzed data. S.C. Huen, A. Wang, K. Feola, R. Desrouleaux, and H.H. Luan conducted experiments and acquired data with assistance from R. Hogg and C. Zhang. S.C. Huen and R. Medzhitov wrote the manuscript. Q.J. Zhang performed the echocardiography studies, and Q.J. Zhang and Z.P. Liu analyzed the echocardiography data.

Disclosures: H.H. Luan reported "other" from NGM Biopharmaceuticals outside the submitted work. No other disclosures were reported.

Submitted: 6 October 2020 Revised: 22 June 2021 Accepted: 2 August 2021

References

Adamo, S.A. 2005. Parasitic suppression of feeding in the tobacco hornworm, Manduca sexta: parallels with feeding depression after an immune challenge. Arch. Insect Biochem. Physiol. 60:185-197. https://doi.org/10 .1002/arch.20068

Adams, A.C., C.C. Cheng, T. Coskun, and A. Kharitonenkov. 2012. FGF21 requires βklotho to act in vivo. *PLoS One.* 7:e49977. https://doi.org/10.1371/journal.pone.0049977

Ahmad, S., A. Tejuja, K.D. Newman, R. Zarychanski, and A.J. Seely. 2009. Clinical review: a review and analysis of heart rate variability and the diagnosis and prognosis of infection. Crit. Care. 13:232. https://doi.org/ 10.1186/cc8132

Ameka, M., K.R. Markan, D.A. Morgan, L.D. BonDurant, S.O. Idiga, M.C. Naber, Z. Zhu, L.V. Zingman, J.L. Grobe, K. Rahmouni, and M.J. Potthoff. 2019. Liver Derived FGF21 Maintains Core Body Temperature During Acute Cold Exposure. Sci. Rep. 9:630. https://doi.org/10.1038/s41598-018-37198-y

Ayres, J.S., and D.S. Schneider. 2009. The role of anorexia in resistance and tolerance to infections in Drosophila. PLoS Biol. 7:e1000150. https://doi.org/10.1371/journal.pbio.1000150

Ayres, J.S., and D.S. Schneider. 2012. Tolerance of infections. Annu. Rev. Immunol. 30:271-294. https://doi.org/10.1146/annurev-immunol-020711-075030

Badman, M.K., P. Pissios, A.R. Kennedy, G. Koukos, J.S. Flier, and E. Maratos-Flier. 2007. Hepatic fibroblast growth factor 21 is regulated by PPARalpha and is a key mediator of hepatic lipid metabolism in ketotic states. Cell Metab. 5:426-437. https://doi.org/10.1016/j.cmet.2007.05.002

BonDurant, L.D., M. Ameka, M.C. Naber, K.R. Markan, S.O. Idiga, M.R. Acevedo, S.A. Walsh, D.M. Ornitz, and M.J. Potthoff. 2017. FGF21 Regulates Metabolism Through Adipose-Dependent and -Independent Mechanisms. Cell Metab. 25:935–944.e4. https://doi.org/10.1016/j.cmet.2017.03.005

Bookout, A.L., M.H.M. de Groot, B.M. Owen, S. Lee, L. Gautron, H.L. Lawrence, X. Ding, J.K. Elmquist, J.S. Takahashi, D.J. Mangelsdorf, and S.A. Kliewer. 2013. FGF21 regulates metabolism and circadian behavior by acting on the nervous system. *Nat. Med.* 19:1147–1152. https://doi.org/10.1038/nm.3249

Casscells, W., M.F. Vasseghi, M.S. Siadaty, M. Madjid, H. Siddiqui, B. Lal, and S. Payvar. 2005. Hypothermia is a bedside predictor of imminent death in patients with congestive heart failure. Am. Heart J. 149:927–933. https://doi.org/10.1016/j.ahj.2004.07.038

Coate, K.C., G. Hernandez, C.A. Thorne, S. Sun, T.D.V. Le, K. Vale, S.A. Kliewer, and D.J. Mangelsdorf. 2017. FGF21 Is an Exocrine Pancreas



- Secretagogue. Cell Metab. 25:472-480. https://doi.org/10.1016/j.cmet
- Coote, J.H., and K.M. Spyer. 2018. Central control of autonomic function.

 Brain Neurosci. Adv. 2:2398212818812012. https://doi.org/10.1177/
 2398212818812012
- Ding, X., J. Boney-Montoya, B.M. Owen, A.L. Bookout, K.C. Coate, D.J. Mangelsdorf, and S.A. Kliewer. 2012. βKlotho is required for fibroblast growth factor 21 effects on growth and metabolism. *Cell Metab.* 16: 387–393. https://doi.org/10.1016/j.cmet.2012.08.002
- Domouzoglou, E.M., F.M. Fisher, I. Astapova, E.C. Fox, A. Kharitonenkov, J.S. Flier, A.N. Hollenberg, and E. Maratos-Flier. 2014. Fibroblast growth factor 21 and thyroid hormone show mutual regulatory dependency but have independent actions in vivo. *Endocrinology*. 155:2031–2040. https://doi.org/10.1210/en.2013-1902
- Drosatos, K., A. Lymperopoulos, P.J. Kennel, N. Pollak, P.C. Schulze, and I.J. Goldberg. 2015. Pathophysiology of sepsis-related cardiac dysfunction: driven by inflammation, energy mismanagement, or both? *Curr. Heart Fail. Rep.* 12:130–140. https://doi.org/10.1007/s11897-014-0247-z
- Ebrahimi, F., C. Wolffenbuttel, C.A. Blum, C. Baumgartner, B. Mueller, P. Schuetz, C. Meier, M. Kraenzlin, M. Christ-Crain, and M.J. Betz. 2019. Fibroblast growth factor 21 predicts outcome in community-acquired pneumonia: secondary analysis of two randomised controlled trials. *Eur. Respir. J.* 53:1800973. https://doi.org/10.1183/13993003.00973-2018
- Fairchild, K.D., J.J. Saucerman, L.L. Raynor, J.A. Sivak, Y. Xiao, D.E. Lake, and J.R. Moorman. 2009. Endotoxin depresses heart rate variability in mice: cytokine and steroid effects. Am. J. Physiol. Regul. Integr. Comp. Physiol. 297:R1019-R1027. https://doi.org/10.1152/ajpregu.00132.2009
- Fairchild, K.D., V. Srinivasan, J.R. Moorman, R.P. Gaykema, and L.E. Goehler. 2011. Pathogen-induced heart rate changes associated with cholinergic nervous system activation. Am. J. Physiol. Regul. Integr. Comp. Physiol. 300:R330-R339. https://doi.org/10.1152/ajpregu.00487.2010
- Feingold, K.R., C. Grunfeld, J.G. Heuer, A. Gupta, M. Cramer, T. Zhang, J.K. Shigenaga, S.M. Patzek, Z.W. Chan, A. Moser, et al. 2012. FGF21 is increased by inflammatory stimuli and protects leptin-deficient ob/ob mice from the toxicity of sepsis. *Endocrinology*. 153:2689–2700. https://doi.org/10.1210/en.2011-1496
- Fisher, F.M., and E. Maratos-Flier. 2016. Understanding the Physiology of FGF21. *Annu. Rev. Physiol.* 78:223–241. https://doi.org/10.1146/annurev-physiol-021115-105339
- Fisher, F.M., S. Kleiner, N. Douris, E.C. Fox, R.J. Mepani, F. Verdeguer, J. Wu, A. Kharitonenkov, J.S. Flier, E. Maratos-Flier, and B.M. Spiegelman. 2012. FGF21 regulates PGC-1α and browning of white adipose tissues in adaptive thermogenesis. Genes Dev. 26:271–281. https://doi.org/10.1101/gad.177857.111
- Gariani, K., G. Drifte, I. Dunn-Siegrist, J. Pugin, and F.R. Jornayvaz. 2013. Increased FGF21 plasma levels in humans with sepsis and SIRS. Endocr. Connect. 2:146-153. https://doi.org/10.1530/EC-13-0040
- Goldberger, J.J. 1999. Sympathovagal balance: how should we measure it? Am. J. Physiol. 276:H1273-H1280. https://doi.org/10.1152/ajpheart.1999.276.4
- Grimaud, J., and V.N. Murthy. 2018. How to monitor breathing in laboratory rodents: a review of the current methods. J. Neurophysiol. 120:624–632. https://doi.org/10.1152/jn.00708.2017
- Hermann, G.E., M.J. Barnes, and R.C. Rogers. 2006. Leptin and thyrotropinreleasing hormone: cooperative action in the hindbrain to activate brown adipose thermogenesis. *Brain Res.* 1117:118–124. https://doi.org/10 .1016/j.brainres.2006.08.018
- Hernandez, G., T. Luo, T.A. Javed, L. Wen, M.A. Kalwat, K. Vale, F. Ammouri, S.Z. Husain, S.A. Kliewer, and D.J. Mangelsdorf. 2020. Pancreatitis is an FGF21-deficient state that is corrected by replacement therapy. *Sci. Transl. Med.* 12:eaay5186. https://doi.org/10.1126/scitranslmed.aay5186
- Hill, C.M., T. Laeger, M. Dehner, D.C. Albarado, B. Clarke, D. Wanders, S.J. Burke, J.J. Collier, E. Qualls-Creekmore, S.M. Solon-Biet, et al. 2019. FGF21 Signals Protein Status to the Brain and Adaptively Regulates Food Choice and Metabolism. Cell Rep. 27:2934–2947.e3. https://doi.org/10.1016/j.celrep.2019.05.022
- Holland, W.L., A.C. Adams, J.T. Brozinick, H.H. Bui, Y. Miyauchi, C.M. Kusminski, S.M. Bauer, M. Wade, E. Singhal, C.C. Cheng, et al. 2013. An FGF21-adiponectin-ceramide axis controls energy expenditure and insulin action in mice. *Cell Metab.* 17:790–797. https://doi.org/10.1016/j.cmet.2013.03.019
- Inagaki, T., P. Dutchak, G. Zhao, X. Ding, L. Gautron, V. Parameswara, Y. Li, R. Goetz, M. Mohammadi, V. Esser, et al. 2007. Endocrine regulation of the fasting response by PPARalpha-mediated induction of fibroblast growth factor 21. Cell Metab. 5:415–425. https://doi.org/10.1016/j.cmet.2007.05.003
- Kim, A.M., V.R. Somayaji, J.Q. Dong, T.P. Rolph, Y. Weng, J.R. Chabot, K.E. Gropp, S. Talukdar, and R.A. Calle. 2017. Once-weekly administration of

- a long-acting fibroblast growth factor 21 analogue modulates lipids, bone turnover markers, blood pressure and body weight differently in obese people with hypertriglyceridaemia and in non-human primates. Diabetes Obes. Metab. 19:1762–1772. https://doi.org/10.1111/dom.13023
- Kong, B., J. Huang, Y. Zhu, G. Li, J. Williams, S. Shen, L.M. Aleksunes, J.R. Richardson, U. Apte, D.A. Rudnick, and G.L. Guo. 2014. Fibroblast growth factor 15 deficiency impairs liver regeneration in mice. Am. J. Physiol. Gastrointest. Liver Physiol. 306:G893–G902. https://doi.org/10.1152/ajpgi.00337.2013
- Kurosu, H., M. Choi, Y. Ogawa, A.S. Dickson, R. Goetz, A.V. Eliseenkova, M. Mohammadi, K.P. Rosenblatt, S.A. Kliewer, and M. Kuro-O. 2007. Tissue-specific expression of betaKlotho and fibroblast growth factor (FGF) receptor isoforms determines metabolic activity of FGF19 and FGF21. J. Biol. Chem. 282:26687-26695. https://doi.org/10.1074/jbc.M704165200
- Lan, T., D.A. Morgan, K. Rahmouni, J. Sonoda, X. Fu, S.C. Burgess, W.L. Holland, S.A. Kliewer, and D.J. Mangelsdorf. 2017. FGF19, FGF21, and an FGFR1/β-Klotho-Activating Antibody Act on the Nervous System to Regulate Body Weight and Glycemia. *Cell Metab.* 26:709–718.e3. https://doi.org/10.1016/j.cmet.2017.09.005
- Li, X., Z. Zhu, T. Zhou, X. Cao, T. Lu, Y. Liang, J. He, C. Liu, Z. Dou, and B. Shen. 2018. Early increases in serum FGF21 levels predict mortality of septic patients. *Cytokine*. 111:428–433. https://doi.org/10.1016/j.cyto.2018.05.020
- Liang, Q., L. Zhong, J. Zhang, Y. Wang, S.R. Bornstein, C.R. Triggle, H. Ding, K.S. Lam, and A. Xu. 2014. FGF21 maintains glucose homeostasis by mediating the cross talk between liver and brain during prolonged fasting. Diabetes. 63:4064–4075. https://doi.org/10.2337/db14-0541
- Liu, S.Q., D. Roberts, A. Kharitonenkov, B. Zhang, S.M. Hanson, Y.C. Li, L.Q. Zhang, and Y.H. Wu. 2013. Endocrine protection of ischemic myocardium by FGF21 from the liver and adipose tissue. Sci. Rep. 3:2767. https://doi.org/10.1038/srep02767
- Medina, E. 2010. Murine model of polymicrobial septic peritonitis using cecal ligation and puncture (CLP). Methods Mol. Biol. 602:411-415. https://doi .org/10.1007/978-1-60761-058-8_23
- Medzhitov, R., D.S. Schneider, and M.P. Soares. 2012. Disease tolerance as a defense strategy. Science. 335:936-941. https://doi.org/10.1126/science 1214935
- Murray, M.J., and A.B. Murray. 1979. Anorexia of infection as a mechanism of host defense. Am. J. Clin. Nutr. 32:593–596. https://doi.org/10.1093/ajcn/ 32.3.593
- Nautiyal, K.M., M. Dailey, N. Brito, M.N. Brito, R.B. Harris, T.J. Bartness, and H.J. Grill. 2008. Energetic responses to cold temperatures in rats lacking forebrain-caudal brain stem connections. Am. J. Physiol. Regul. Integr. Comp. Physiol. 295:R789–R798. https://doi.org/10.1152/ajpregu .90394.2008
- Ogawa, Y., H. Kurosu, M. Yamamoto, A. Nandi, K.P. Rosenblatt, R. Goetz, A.V. Eliseenkova, M. Mohammadi, and M. Kuro-o. 2007. BetaKlotho is required for metabolic activity of fibroblast growth factor 21. *Proc. Natl. Acad. Sci. USA.* 104:7432–7437. https://doi.org/10.1073/pnas.0701600104
- Owen, B.M., A.L. Bookout, X. Ding, V.Y. Lin, S.D. Atkin, L. Gautron, S.A. Kliewer, and D.J. Mangelsdorf. 2013. FGF21 contributes to neuroendocrine control of female reproduction. *Nat. Med.* 19:1153–1156. https://doi.org/10.1038/nm.3250
- Owen, B.M., X. Ding, D.A. Morgan, K.C. Coate, A.L. Bookout, K. Rahmouni, S.A. Kliewer, and D.J. Mangelsdorf. 2014. FGF21 acts centrally to induce sympathetic nerve activity, energy expenditure, and weight loss. *Cell Metab.* 20:670–677. https://doi.org/10.1016/j.cmet.2014.07.012
- Patel, V., R. Adya, J. Chen, M. Ramanjaneya, M.F. Bari, S.K. Bhudia, E.W. Hillhouse, B.K. Tan, and H.S. Randeva. 2014. Novel insights into the cardio-protective effects of FGF21 in lean and obese rat hearts. PLoS One. 9:e87102. https://doi.org/10.1371/journal.pone.0087102
- Patel, R., A.L. Bookout, L. Magomedova, B.M. Owen, G.P. Consiglio, M. Shimizu, Y. Zhang, D.J. Mangelsdorf, S.A. Kliewer, and C.L. Cummins. 2015. Glucocorticoids regulate the metabolic hormone FGF21 in a feed-forward loop. *Mol. Endocrinol.* 29:213–223. https://doi.org/10.1210/me.2014-1259
- Planavila, A., I. Redondo, E. Hondares, M. Vinciguerra, C. Munts, R. Iglesias, L.A. Gabrielli, M. Sitges, M. Giralt, M. van Bilsen, and F. Villarroya. 2013. Fibroblast growth factor 21 protects against cardiac hypertrophy in mice. Nat. Commun. 4:2019. https://doi.org/10.1038/ncomms3019
- Potthoff, M.J., T. Inagaki, S. Satapati, X. Ding, T. He, R. Goetz, M. Mohammadi, B.N. Finck, D.J. Mangelsdorf, S.A. Kliewer, and S.C. Burgess. 2009. FGF21 induces PGC-1alpha and regulates carbohydrate and fatty acid metabolism during the adaptive starvation response. Proc. Natl.



- Acad. Sci. USA. 106:10853-10858. https://doi.org/10.1073/pnas.0904187106
- Potthoff, M.J., S.A. Kliewer, and D.J. Mangelsdorf. 2012. Endocrine fibroblast growth factors 15/19 and 21: from feast to famine. *Genes Dev.* 26:312–324. https://doi.org/10.1101/gad.184788.111
- Premer, C., A.J. Kanelidis, J.M. Hare, and I.H. Schulman. 2019. Rethinking Endothelial Dysfunction as a Crucial Target in Fighting Heart Failure. Mayo Clin. Proc. Innov. Qual. Outcomes. 3:1–13. https://doi.org/10.1016/j.mayocpiqo.2018.12.006
- Price, C.J., T.D. Hoyda, and A.V. Ferguson. 2008. The area postrema: a brain monitor and integrator of systemic autonomic state. *Neuroscientist*. 14: 182–194. https://doi.org/10.1177/1073858407311100
- Rao, S., A.M.P. Schieber, C.P. O'Connor, M. Leblanc, D. Michel, and J.S. Ayres. 2017. Pathogen-Mediated Inhibition of Anorexia Promotes Host Survival and Transmission. Cell. 168:503–516.e12. https://doi.org/10.1016/j.cell.2017.01.006
- Singer, M., C.S. Deutschman, C.W. Seymour, M. Shankar-Hari, D. Annane, M. Bauer, R. Bellomo, G.R. Bernard, J.D. Chiche, C.M. Coopersmith, et al. 2016. The Third International Consensus Definitions for Sepsis and Septic Shock (Sepsis-3). JAMA. 315:801-810. https://doi.org/10.1001/jama.2016.0287
- Soares, M.P., R. Gozzelino, and S. Weis. 2014. Tissue damage control in disease tolerance. Trends Immunol. 35:483-494. https://doi.org/10.1016/j.it..2014.08.001
- Song, P., C. Zechner, G. Hernandez, J. Cánovas, Y. Xie, V. Sondhi, M. Wagner, V. Stadlbauer, A. Horvath, B. Leber, et al. 2018. The Hormone FGF21 Stimulates Water Drinking in Response to Ketogenic Diet and Alcohol. Cell Metab. 27:1338-1347.e4. https://doi.org/10.1016/j.cmet.2018.04.001
- Talukdar, S., B.M. Owen, P. Song, G. Hernandez, Y. Zhang, Y. Zhou, W.T. Scott, B. Paratala, T. Turner, A. Smith, et al. 2016. FGF21 Regulates

- Sweet and Alcohol Preference. *Cell Metab.* 23:344–349. https://doi.org/10.1016/j.cmet.2015.12.008
- Toscano, M.G., D. Ganea, and A.M. Gamero. 2011. Cecal ligation puncture procedure. J. Vis. Exp. (51):2860. https://doi.org/10.3791/2860
- Turner, T., X. Chen, M. Zahner, A. Opsahl, G. DeMarco, M. Boucher, B. Goodwin, and M. Perreault. 2018. FGF21 increases water intake, urine output and blood pressure in rats. PLoS One. 13:e0202182. https://doi.org/10.1371/journal.pone.0202182
- Van Wyngene, L., J. Vandewalle, and C. Libert. 2018. Reprogramming of basic metabolic pathways in microbial sepsis: therapeutic targets at last? EMBO Mol. Med. 10:e8712. https://doi.org/10.15252/emmm.201708712
- Vaseghi, M., and K. Shivkumar. 2008. The role of the autonomic nervous system in sudden cardiac death. Prog. Cardiovasc. Dis. 50:404–419. https://doi.org/10.1016/j.pcad.2008.01.003
- Wang, A., S.C. Huen, H.H. Luan, S. Yu, C. Zhang, J.D. Gallezot, C.J. Booth, and R. Medzhitov. 2016. Opposing Effects of Fasting Metabolism on Tissue Tolerance in Bacterial and Viral Inflammation. Cell. 166:1512–1525.e12. https://doi.org/10.1016/j.cell.2016.07.026
- Wang, A., S.C. Huen, H.H. Luan, K. Baker, H. Rinder, C.J. Booth, and R. Medzhitov. 2018. Glucose metabolism mediates disease tolerance in cerebral malaria. Proc. Natl. Acad. Sci. USA. 115:11042-11047. https://doi.org/10.1073/pnas.1806376115
- Weis, S., A.R. Carlos, M.R. Moita, S. Singh, B. Blankenhaus, S. Cardoso, R. Larsen, S. Rebelo, S. Schäuble, L. Del Barrio, et al. 2017. Metabolic Adaptation Establishes Disease Tolerance to Sepsis. Cell. 169:1263–1275.e14. https://doi.org/10.1016/j.cell.2017.05.031
- Zhang, Y., Y. Xie, E.D. Berglund, K.C. Coate, T.T. He, T. Katafuchi, G. Xiao, M.J. Potthoff, W. Wei, Y. Wan, et al. 2012. The starvation hormone, fibroblast growth factor-21, extends lifespan in mice. *eLife*. 1:e00065. https://doi.org/10.7554/eLife.00065



Supplemental material

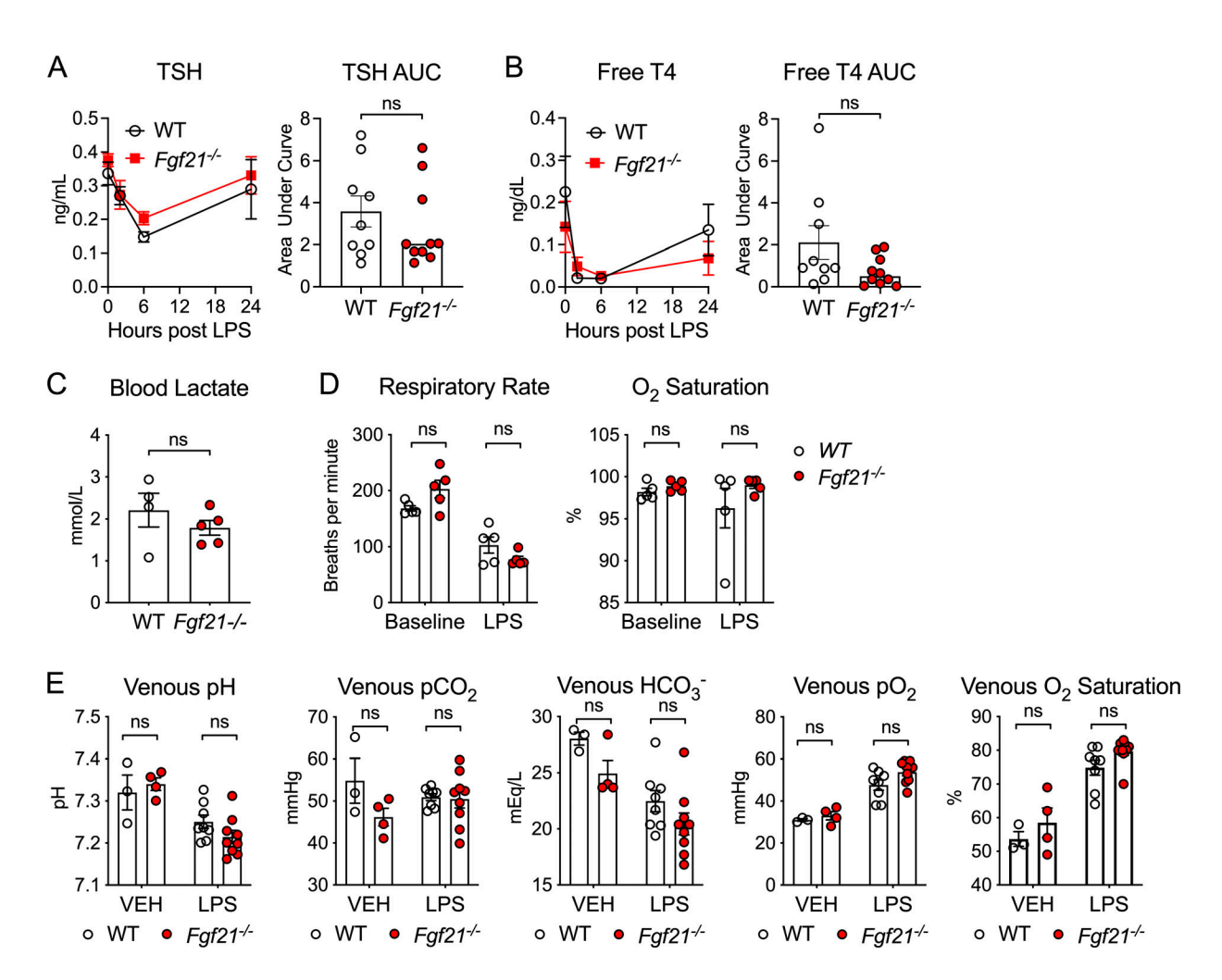


Figure S1. **FGF21-deficient mice do not have defects in thyroid hormone axis or differences in lactate levels or blood gases after LPS challenge. (A and B)** C57BL/6J (WT) and $Fgf21^{-/-}$ mice were challenged with LPS 10 mg/kg i.p., n = 9-10/group; pooled data are from two independent experiments. **(A)** Thyroid-stimulating hormone (TSH) measured by ELISA. **(B)** Free thyroxine (T4) measured by ELISA. **(C)** Venous blood lactate measured by the i-STAT1 Handheld Analyzer CG4+ cartridge 24 h after 12.5 mg/kg i.p. LPS in WT and $Fgf21^{-/-}$ mice; n = 4-5/group. Data are from one of two independent experiments. **(D)** Respiratory rate and O_2 saturation measured before and after LPS challenge in WT and $Fgf21^{-/-}$ mice; n = 5/group. Data are from one of two independent experiments with similar results. **(E)** Venous blood gas measured by the i-STAT 1 Handheld Analyzer CG8+ cartridge 24 h after PBS vehicle (VEH) or 12.5 mg/kg i.p. LPS in WT and $Fgf21^{-/-}$ mice; n = 3-9/group. Pooled data are from two independent experiments. Unpaired two-sided t test (A–C) or two-way ANOVA with Sidak's multiple comparisons test (D and E). Data are expressed as mean t SEM.



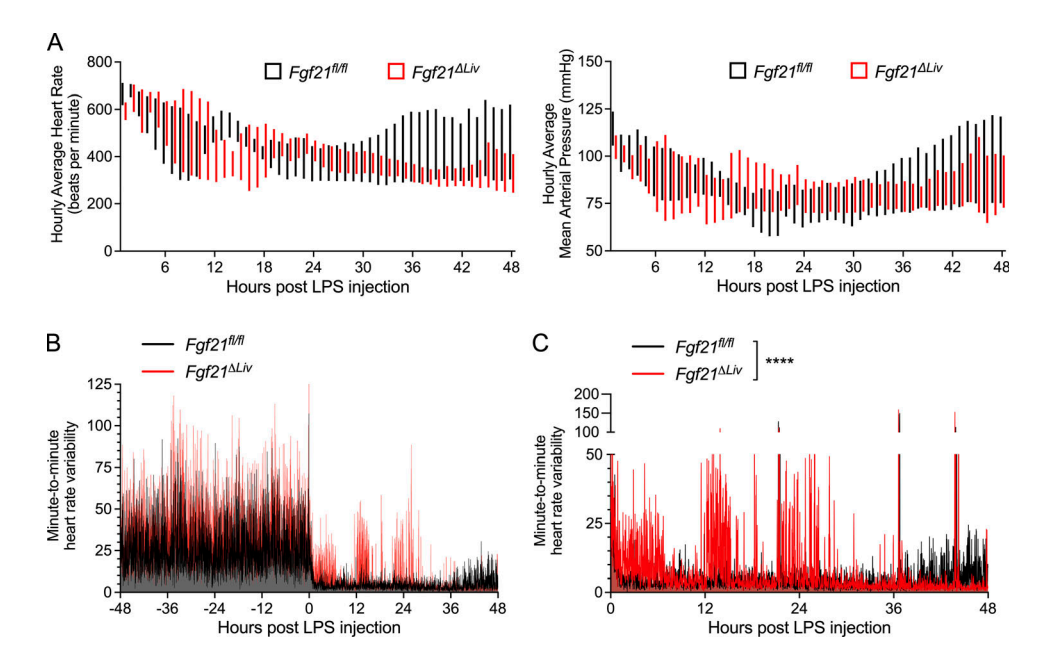


Figure S2. **FGF21 deficiency results in depressed heart rate and increased heart rate variability during endotoxemia.** Ambulatory blood pressure and heart rate measured by in vivo telemetry before and after 2 mg/kg i.p. LPS, related to Fig. 4 D. **(A)** Hourly averages of heart rate and mean arterial pressure after LPS injection in $Fgf21^{fl/fl}$ vs $Fgf21^{\Delta Liv}$. Floating bars represent minimum and maximum hourly averages per genotype group. **(B and C)** Telemetry measurements were recorded every minute. Heart rate differences between each recording are shown. **(B)** Minute-to-minute HRV before and after LPS injection. **(C)** Minute-to-minute HRV after LPS injection, with $Fgf21^{\Delta Liv}$ (red curve) graphed in front to show the difference. n = 4/group; pooled data are from three independent experiments. *****, P < 0.0001, two-way ANOVA. Data are expressed as mean \pm SEM.



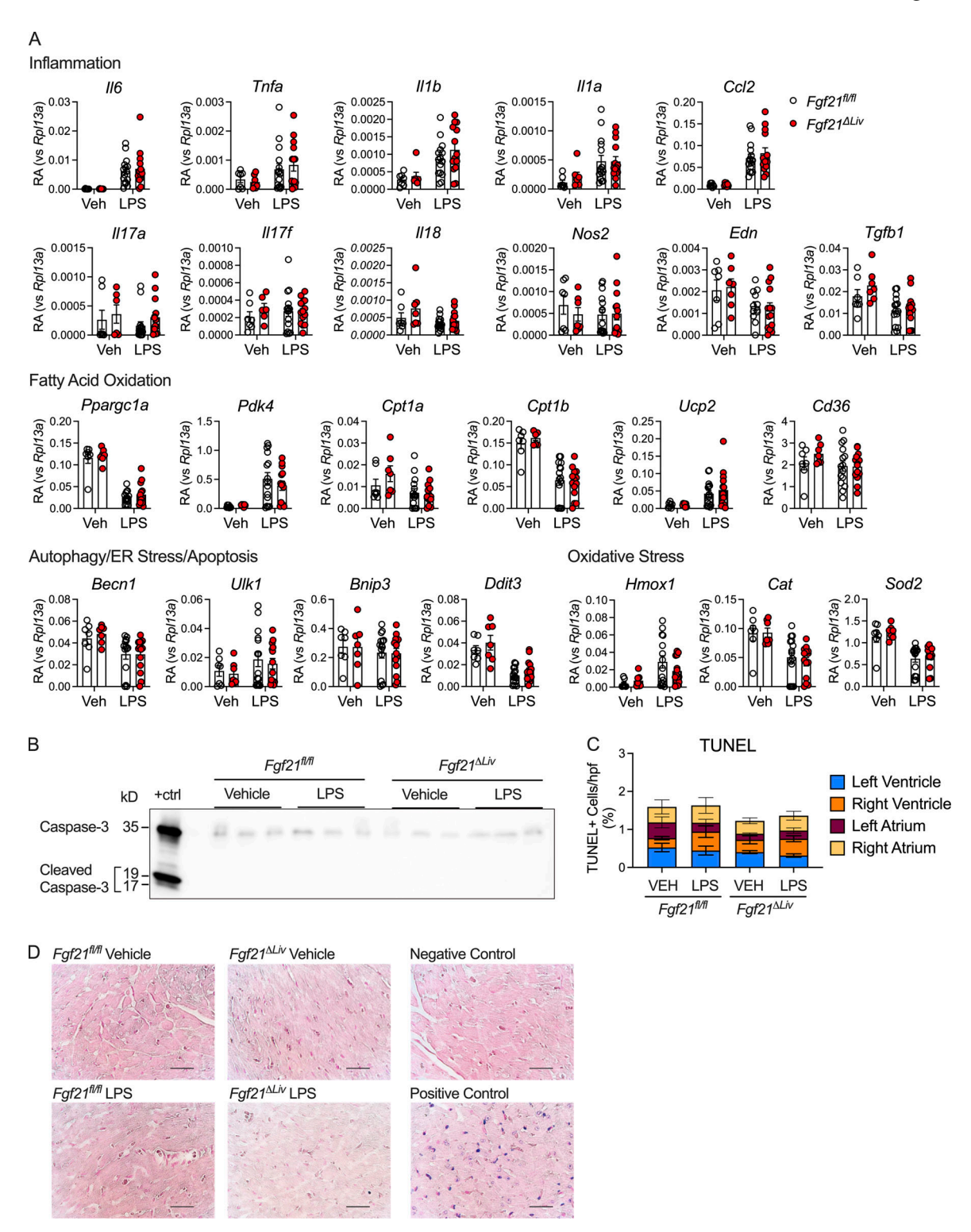


Figure S3. Effects of FGF21 deficiency on cardiac markers of inflammation, fatty acid oxidation, acute stress response, and cell apoptosis during endotoxemia. $Fgf21^{fl/fl}$ and $Alb\text{-}Cre; Fgf21^{fl/fl}$ ($Fgf21^{fl/fl}$) mice given vehicle or 5 mg/kg i.p. LPS treatment, whole heart tissue harvested 20 h after vehicle or LPS treatment. (A) RA of mRNA expression, shown relative to Rpl13a. Vehicle (Veh), n = 7/group; LPS, n = 14-15/group. mRNA data are pooled from four independent experiments. (B) Whole heart tissue protein lysates immunoblotted for caspase-3. Positive control (+ctrl) generated from Hepa1-6 cells treated with 5 μ M staurosporine for 24 h. Representative blot from one of two independent experiments. (C) Quantification of TUNEL-positive cells per 400×-power field. n = 5/vehicle group, n = 6/LPS group; data are pooled from two independent experiments. Data are expressed as mean percentage of TUNEL-positive cells per total cells per high-power field (hpf). (D) Representative images of heart sections from the left ventricle using TACS Blue Labeling to stain TUNEL-positive cells and Nuclear Fast Red heart to stain nuclei. Terminal deoxynucleotidyl transferase enzyme was omitted for the unlabeled negative control. TACS-nuclease treatment was used for the positive control. Scale bars represent 100 μ m. Two-way ANOVA with Sidak's multiple comparisons tests were not statistically significant (A and C). Data are expressed as mean \pm SEM.